Competition and Interplay of Various Intermolecular Interactions in Ultrafast Excited-State Proton and Electron Transfer Reactions

ARTICLE *in* THE JOURNAL OF PHYSICAL CHEMISTRY B · SEPTEMBER 2014

Impact Factor: 3.3 · DOI: 10.1021/jp507390r · Source: PubMed

6 AUTHORS, INCLUDING:

Michael Kuzmin
Lomonosov Moscow State University
59 PUBLICATIONS **576** CITATIONS
SEE PROFILE

Kyril M Solntsev
Georgia Institute of Technology
87 PUBLICATIONS **2,383** CITATIONS
SEE PROFILE

THE JOURNAL OF PHYSICAL CHEMISTRY B

Article

pubs.acs.org/JPCB

Competition and Interplay of Various Intermolecular Interactions in Ultrafast Excited-State Proton and Electron Transfer Reactions

Michael G. Kuzmin,*[,†] Irina V. Soboleva,[†] Vladimir L. Ivanov,[†] Elizabeth-Ann Gould,[‡] Dan Huppert,[§] and Kyril M. Solntsev*[,‡]

[†]Department of Chemistry, Moscow M. V. Lomonosov University, Leninskie Gory, Moscow, 119991, Russia

[‡]School of Chemistry and Biochemistry, Georgia Institute of Technology, 901 Atlantic Drive, Atlanta, Georgia 30332-0400, United States

[§]Raymond and Beverly Sackler Faculty of Exact Sciences, School of Chemistry, Tel Aviv University, Tel Aviv 69978, Israel

ABSTRACT: The main features of the photoinduced kinetics of both ultrafast excited-state proton and electron transfer reactions that occur in the picosecond (ps) and femtosecond (fs) time domains are compared. Proton transfer (PT) reaction kinetics can be described in terms of several discrete values of rate coefficients in the form of polyexponential functions where each value of the rate coefficient can be attributed to a definite physical behavior of the reaction mechanism. In contrast, electron transfer (ET) reaction kinetics requires a consideration of a continuous distribution of rate coefficients. This difference can be related to structure of the ground-state reactant pairs for each reaction. Excited-state ET can occur at various configurations of reactant molecules and its rate reflects the fluctuations of the distances and orientations of these molecules. In contrast, excited-state PT requires preliminary formation of a ground-state H-bonded complex with definite structure where the reaction occurs after photoexcitation.

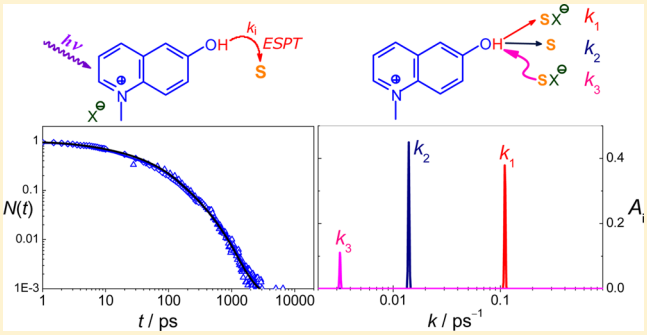

INTRODUCTION

Proton transfer (PT) and electron transfer (ET) are very important steps in the mechanisms of various chemical and biological processes, in medicine, and in chemical technology.[1−5] These reactions are the fastest bimolecular chemical reactions since they involve only small changes of nuclear coordinates of the reactant molecules. The goal of this work is to analyze the similarities and dissimilarities of the ultrafast kinetics of ET and PT reactions in liquid solutions. Important differences between these reactions can be expected to arise because of the 1000-fold difference between the mass of an electron and a proton and also from the asymmetry of the hydrogen bond in the H-bonded complex formed prior to the reaction.

An important concept in chemical kinetics is the rate coefficient. For a unimolecular reaction, the rate coefficient k of a first order kinetics law $dC/dt = -kC$, where C is the concentration of the reactant. However, it should be noticed that even for unimolecular processes the existence of a rate coefficient as a time independent constant is not obvious.[6] Therefore, we will use the term "rate coefficient" throughout the text. Usually in ET and PT reactions, different reaction rates are expected for individual distances between the donor and acceptor. Thus, a single time-independent macroscopic rate coefficient is not anticipated in such a case. The observed macroscopic rate coefficient is an average over many microscopic rates. In the latter case $k = \Sigma_i A_i k_i$, where k_i are rates associated with individual distances and A_i are the corresponding probabilities to be in these distances. The rate coefficient k is therefore time-independent only when the probabilities A_i remain constant during the chemical reaction. The situation in which the relative populations of individual molecular distances remain constant, even if the overall population decays as the reaction proceeds, is sometimes referred to as a quasi-steady state. This occurs only when the relaxation process that keeps the thermal equilibrium between the states is faster than the chemical process studied. In ultrafast PT and ET reactions (in fs−ps range), these relaxation processes occur on a slow time scale ($\tau_L \sim 1-10$ ps, $\tau_{Rot} \sim 20-40$ ps, $\tau_{Diff} = R^2/D \sim 1$ ns for liquid solutions) and do not provide the conditions for a definite steady-state regime, and actually, it is expected that a gradual transformation of the reaction mechanism will take place.

Recently, some of us have shown that the nonexponential kinetics of ultrafast ET reactions in liquid solutions is related to the competition of several rate control factors:[7] (1) the wide distributions of ET rate coefficients $P(k_{ET})$ (for $k_{ET} \approx 0.1-2$

Special Issue: Photoinduced Proton Transfer in Chemistry and Biology Symposium

Received: July 23, 2014
Revised: September 9, 2014
Published: September 10, 2014

   dx.doi.org/10.1021/jp507390r | J. Phys. Chem. B 2015, 119, 2444−2453

ps^{-1}) caused by fluctuations of the electronic coupling matrix element (V_{AD}) for reactant molecules located inside in the interior of the solvent shell; (2) reorganization of the medium and reactant molecules (in the range of the dielectric relaxation times); and (3) nonstationary diffusion of the reactant molecules (for $k_{Diff}[Q] \approx 0.001-0.03$ ps^{-1}). In viscous solvents ($\eta > 5$ cP), some contribution of electron tunneling outside the interior of the solvent shell is also possible. This was shown using the rate distribution approach in which $P(k_{ET})$ is obtained directly from the experimental kinetics of various ultrafast excited-state ET (ESET) reactions. In this paper we used a similar approach to reveal the physical behavior of the nonexponential kinetics of ultrafast excited-state PT (ESPT) reactions and compare mechanisms and main features of PT and ET reactions.

EXPERIMENTS AND METHODS

Data Management. In this paper we analyzed the numeric kinetic data of the excited-state PT and ET published earlier in refs 8−11, which also included all details on the sample preparation and the experimental techniques used. All data were collected using the fluorescence upconversion technique with femtosecond resolution and the time-correlated single photon counting technique. ESPT data collected and analyzed by some of us[8,9] dealt with the protolytic photodissociation of *N*-methyl-6-hydroxyquinolinium (MHQ) nonaflate (nonafluorobutanesulfonate) in water and various alcohols. The ESET numeric data on perylene derivatives in various solvents[10,11] was kindly provided by Prof. Eric Vauthey (University of Geneva). The fluorescence kinetic data were fit with multiexponential or multihyperbolic (see eq 6 below) expressions after deconvolution. The fitting error is embedded in the number of significant figures and is between 5−10% for all lifetime values. Chemical structures of all fluorophores studied in this paper are presented in Scheme 1.

Scheme 1. Chemical Structure and the Abbreviations of the Fluorophores Studied in This Paper

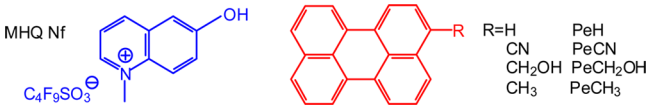

Rate Distributions *P*(*k*). In this work we compare some important features of ultrafast ESPT and ESET reactions using both the traditional and the rate distribution approaches.[7] The rate distribution approach was shown to provide a convenient method for the analysis of complex kinetics of ultrafast reactions when the reaction rate control factors undergo transformations during the course of the reaction. In this approach the reaction kinetics is represented by the reaction rate distribution function, $P(k)$:

$$N(t)/N(0) = \int_0^\infty P(k)\ \exp(-kt)\mathrm{d}k \tag{1}$$

The rate distribution $P(k)$ for a given system consists of a single band or several bands and represents some kind of a "rate spectrum". This approach is much more informative than traditional forms of presenting experimental kinetics in the form of $N(t)/N(0)$ as a sum of exponential functions or the time dependent rate coefficient which all have rather smooth shape. These bands usually correspond to different rate control factors. Total "rate spectrum" demonstrates what kinds of molecular mobility and solvent dynamics (e.g., electronic coupling, reorientation of the reactant molecules, translational diffusion, electron tunneling, etc.) are responsible for actual changes of the reaction rate by simple comparison of the rates observed in the given system with typical rates of molecular mobility and solvent dynamics.

There are several fitting procedures for recovery of the distribution of rate coefficients $P(k)$ (a Laplace original) from the experimental kinetics $N(t)/N(0)$ (a Laplace image).[7,12−14] In a general case, the direct inversion of the Laplace transform for recovering of the arbitrary probability densities of the rate coefficients $P(k)$ has serious shortcomings, related to numerical instability, when the experimental data are intrinsically noisy.[13,14] This is related with a general property of inverse Laplace transform−the inverse transform of an experimental data set, which is inevitably incomplete and noisy, leads to ambiguity in $P(k)$. A multitude of distribution functions will agree equally well with the experimental data. A sophisticated inversion method employs the maximum entropy method,[14] a data analysis technique that has found wide application in various fields. But in many chemical systems this problem can be simplified considerably, and the total rather wide kinetic rate spectrum can be presented as a sum of several bands $P_\Sigma(k) = \sum_i A_i\ P_i(k)$, using the property of the additivity of the Laplace transform (total $P_\Sigma(k) = a_1\ P_1(k) + a_2\ P_2(k)$ when $N_\Sigma(t)/N(0) = a_1\ N_1(t) + a_2\ N_2(t)$). Each component can have different $P_i(k)$ and $N_i(t)$, depending on the physical behavior of the rate control factor. This method of the model functions was found to provide the results with similar accuracy using more simple mathematical procedures.[7]

Polyexponential presentation of the reaction kinetics formally implies some combination of several chemical reactions with fixed values of rate coefficients and amplitudes and exponential kinetics of each reaction. For instance, simple reversible ESPT reactions or exciplex formation can be described by biexponential kinetics expressions:

$$N(t)/N(0) = \alpha\ \exp(-t/\tau_1) + (1 - \alpha)\ \exp(-t/\tau_2) \tag{2}$$

$$N'(t)/N(0) = (k_{-1}/(1/\tau_1 - 1/\tau_2))(\exp(-t/\tau_2) - \exp(-t/\tau_1)) \tag{3}$$

where $N(t)$ and $N'(t)$ are concentrations of the initially excited form (photoacid *ROH or monomer *M) and of the product (excited conjugate base $*RO^-$ or exciplex), respectively,

$$1/\tau_{1,2} = (1/\tau_0 + k_1[B] + 1/\tau'_0 + k_{-1}[HB^+])/2 \pm \{(1/\tau_0 + k_1[B] - 1/\tau'_0 - k_{-1}[HB^+])^2/4 + k_{-1}[HB^+]k_1[B]\}^{1/2} \tag{4}$$

$$\alpha = (1/\tau_0 + k_1[B] - 1/\tau_2)/(1/\tau_1 - 1/\tau_2) \tag{5}$$

τ_0 and τ'_0 are lifetimes of *ROH (or *M) and $*RO^-$ (or exciplex), k_1 and k_{-1} are rate coefficients of the forward and back reactions, [B] and $[HB^+]$ are concentrations of the reactant and its protonated form. The rate distribution functions $P(k)$ in the case of polyexponential decay have a form of δ-functions with several values of rate coefficients k_i and areas proportional to A_i.

Many ultrafast reactions cannot be described by fixed values of rate coefficients since these rates depend on several factors,

dx.doi.org/10.1021/jp507390r | J. Phys. Chem. B 2015, 119, 2444−2453

such as the distribution of distances between the reactant molecules ($P(R_{AD})$) and their mutual orientation ($P(\theta, \phi)$),[15] electronic coupling matrix element ($P(V_{AD})$),[16−19] and so on. In such cases one has to use the continuous distribution $P(k)$. To obtain $P(k)$ in the form of a continuous function one has to express $N(t)/N(0) = \sum_i A_i N_i(t)$ as the sum of some functions that have the Laplace originals in the form of continuous functions $P_i(k)$. For instance, the Laplace original $P(\ln k) = (k/\gamma_i)^m \exp(-k/\gamma_i)/(m-1)!$ (corresponding to the Laplace image $N_i(t) = 1/(1+\gamma_i t)^m$) is close to a Gaussian distribution $P(\ln k) = (1/\sigma(2\pi)^{1/2}) \exp(-(\ln k - \ln k_0)^2/2\sigma^2)$ with $\sigma = 0.3-0.5$.[7] When $P_i(k)$ for each rate control factor is close to a Gaussian distribution then total experimental kinetics can be approximated by a sum of Laplace images specific for those mechanisms in the form of hyperbolic functions:

$$N_\Sigma(t)/N(0) = \sum_i A_i/(1+\gamma_i t)^m \tag{6}$$

In such a case, all the parameters A_1 and γ_i can be obtained directly from the experimental kinetics using any kind of standard mathematical software package.

It should be mentioned that, in the case of continuous distributions $P(k)$, the usual presentation of the experimental data on nonexponential kinetics in the form of polyexponential functions $N(t)/N(0) = \sum_i A_i \exp(-k_i t)$ is not convenient to describe the distribution $P(k)$. This is because an inverse Laplace transform of the exponential function is a δ-function, and one obtains only several amplitudes for discrete (sometimes rather arbitrary) values of k_i. In the case of hyperbolic approximation (2), one obtains $P(k)$ in the form of continuous functions

$$P(k) = \sum_i A_i (k^{m-1}/\gamma_i^m) \exp(-k/\gamma_i)/(m-1)! \tag{7}$$

or

$$P(\ln k) = \sum_i A_i (k/\gamma_n)^m \exp(-k/\gamma_n)/(m-1)! \tag{8}$$

Both distribution functions 7 and 8 are normalized in coordinates $P(k)$ versus k and $P(\ln k)$ versus $\ln k$, respectively. The width of the distribution functions $P(\ln k) = (k/\gamma_n)^m \exp(-k/\gamma_n)/(m-1)!$ with $m = 4-10$ corresponds to a Gaussian distribution with $\sigma \approx 0.5-0.3$ and $k_{max} = 6.0\gamma$ for $m = 6$.

In diluted solutions, the nonstationary diffusion should be taken into account. In such a case, $P(\ln k)$ cannot be described by hyperbolic function 6 or by Gaussian function. The time-dependent rate coefficient for nonstationary diffusion is known to be expressed by the spherical symmetric Smoluchowski equation[19−21]

$$k_{Diff}(t) = 4\pi R_Q D(1 + R_Q/(\pi D t)^{1/2}) \tag{9}$$

where R_Q is a radius of a quenching sphere, D is a diffusion coefficient. In this case, the diffusion controlled kinetics can be described as

$$N(t)/N(0) = \exp(-C_Q 4\pi R_Q D(1 + R_Q/(\pi D t)^{1/2})t) = \exp(-C_Q 4\pi R_Q D t) \exp(-C_Q 4\pi^{1/2} R_Q{}^2 \times D^{1/2} t^{1/2}) \tag{10}$$

where $C_Q = 0.6[Q]$ is the quencher concentration in molecules nm^{-3}. That corresponds to the Laplace original (at $k_{Diff} \geq 4\pi R_Q D$)

$$P(\ln(C_Q k_{Diff})) = (k_{2D}/2(\pi(k_{Diff} - k_{1D})^3)^{1/2}) \exp(-k_{2D}{}^2/4(k_{Diff} - k_{1D}))/k_{Diff} \tag{11}$$

where $k_{1D} = C_Q 4\pi R_Q D$ and $k_{2D} = C_Q 4\pi^{1/2} R_Q{}^2 D^{1/2}$. This distribution function is normalized in coordinates $P(\ln(C_Q k_{Diff}))$ versus $\ln k$ and has a narrow maximum at stationary value of pseudounimolecular diffusion rate coefficient $k = C_Q k_{Diff} = C_Q 4\pi R_Q D$ and long tail for higher values of k, corresponding to nonstationary diffusion at short times (short distances). The combination of hyperbolic decay and nonstationary diffusion can be described by

$$N(t)/N(0) = A_1/(1+\gamma_1 t)^6 + A_2/(1+\gamma_2 t)^6 + A_3 \exp(-C_Q 4\pi R_Q D(1 + R_Q/(\pi D t)^{1/2})t) \tag{12}$$

and

$$P(\ln k) = A_1(k/\gamma_1)^6 \exp(-k/\gamma_1)/120 + A_2(k/\gamma_2)^6 \exp(-k/\gamma_2)/120 + A_3(k_{2D}/2(\pi(k_{Diff} - k_{1D})^3)^{1/2}) \exp(-k_{2D}{}^2/4(k_{Diff} - k_{1D}))/k_{Diff} \tag{13}$$

RESULTS AND DISCUSSION

ESPT Kinetics. The ESPT kinetics of MHQ (for simplicity we abbreviate MHQ Nf to MHQ) in alcohols and in aqueous solutions can be described by PT reactions of excited cation $^+$*R−OH with the solvent (S)

$$\underset{\text{*MHQ}}{{}^+\text{*R−OH}} + \text{S} \rightleftarrows \underset{\text{zwitterion}}{{}^+\text{*R−O}^-} + \text{HS}^+$$

The kinetics of *MHQ decay, $N(t)$, and zwitterion formation and decay, $N'(t)$, for MHQ in n-butanol is shown in Figure 1A. This kinetics can be described by several exponential functions

$$N(t) = A_1 \exp(-k_1 t) + A_2 \exp(-k_2 t) + A_3 \exp(-k_3 t) + A_4 \exp(-k_4 t) \tag{14}$$

$$N'(t) = A_5 \exp(-k_4 t) - A_1 \exp(-k_1 t) - A_2 \exp(-k_2 t) - A_3 \exp(-k_3 t) \tag{15}$$

with parameters A_i and k_i given in Table 1. Figure 1B shows the results obtained in the form of diagrams $P(k)$ and $P'(k)$ versus k. For convenience these $P(k)$ and $P'(k)$ distributions are shown in the form of narrow Gaussian distribution functions

$$P(\log k) = \sum_i A_i \exp(-(\log k_i - \log k_0)^2/2\sigma^2) \tag{16}$$

with the amplitudes A_i and $\sigma \approx 0.005$ rather than as actual δ-functions (in this case, the total area under these Gaussian curves in coordinates $P(\log k)$ vs $\log k$ is smaller than unity and reaches ca. 0.012). Approximation of the *MHQ decay by four hyperbolic functions (eq 6)

$$N(t) = A_1/(1+\gamma_1 t)^6 + A_2/(1+\gamma_2 t)^6 + A_3/(1+\gamma_3 t)^6 + A_4/(1+\gamma_4 t)^6 \tag{17}$$

dx.doi.org/10.1021/jp507390r | J. Phys. Chem. B 2015, 119, 2444−2453

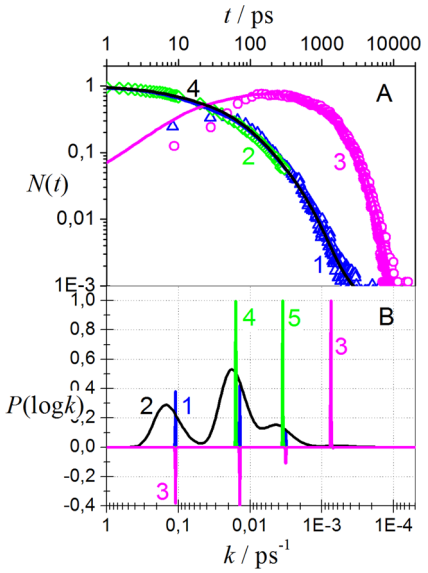

Figure 1. Kinetics of excited-state protolytic dissociation of *MHQ in *n*-BuOH (triangles **1**,[9] lozenges **2**[8]) and zwitterion rise and decay (circles 3[8]; top). Fitting by polyexponential function, eq 14, and by hyperbolic function, eq 17, are shown by solid blue and black lines, respectively. Rate distribution functions $P(\ln k)$ for this reaction (bottom): **1** (blue), polyexponential decay of *MHQ, eq 16; **2** (black), polyhyperbolic decay of *MHQ, eq 18; **3** (magenta), zwitterion polyexponential rise and decay, eq 16 (negative amplitudes correspond to negative values of A_i related to the rise of the zwitterion concentration). Rates of dielectric relaxation ($1/\tau_D$),[8] and diffusion ($k_{Diff} = 4\pi R_{Diff} D$, $R_{Diff} = 0.7$ nm)[8] in *n*-BuOH are shown by green lines in the form of narrow Gaussian functions.[22]

provides similar distributions in the form

$$P(\ln k) = \sum_i A_i (k/\gamma_i)^6 \exp(-k/\gamma_i)/120 \quad (18)$$

shown in Figure 1B by a black line. One can see that this approximation provides results close to poly exponential approximation but with some greater values of $k_i = 6.0\gamma_i$ (see Table 1). The *MHQ decay kinetics contains four positive components, while the kinetics of the zwitterion contains three negative components corresponding to the formation of the zwitterion and one positive component corresponding to its decay (radiative and radiationless). These data indicate the existence of several PT steps in this system: very fast deprotonation with a rate coefficient exceeding the rate of the solvent dielectric relaxation, $1/\tau_D$, deprotonation with a rate coefficient close to $1/\tau_D$, and some slower component.

Similar results were obtained for *MHQ decay in other alcohols and also in aqueous solutions (Figures 2−4). In all alcohols, three components were observed for *MHQ decay (the amplitude of fourth component was very low and this component was ignored previously). In aqueous solutions, only two components have essential amplitudes. The deuterium isotope effect for PT in aqueous solutions was found to be about 3.2 for the faster component ($k = 0.4-1.4$ ps^{-1}) and little smaller (~2.3) for the slower component ($k = 0.15-0.35$ ps^{-1}). It is convenient to use the diagrams of $P(\ln k)$ for the analysis of the reaction mechanism.

Earlier several features of PT mechanisms which can cause deviations from monoexponential kinetics were discussed for various photoacids systems.[21,23,24] The fluorescence decay of strong photoacid 5-cyano-2-naphthol (5CN2OH) exhibits two

Table 1. Kinetic Parameters of Excited-State PT and ET Reactions Obtained by Polyexponential Approximation of Excited MHQ Cation Decay (Eq 14) and by Combination of Hyperbolic Decay and Nonstationary Diffusion (Eq 12) from the Experimental Data[8−11]

				Polyexponential Approximation (Eq 14)						
	*AH (*M)	B (Q)	solvent (η /cP)	A_1	k_1 (ps^{-1})	A_2	k_2 (ps^{-1})	A_3	k_3 (ps^{-1})	τ_D/ps (R_{Diff}) (nm)
1	MHQ[8]	MeOH	MeOH (0.55)	0.46	0.31	0.47	0.059	0.09	0.013	5 (1.2)
2	MHQ[8]	EtOH	EtOH (1.1)	0.30	0.20	0.52	0.051	0.20	0.012	16 (1.0)
3	MHQ[8]	*n*-PrOH	*n*-PrOH (2.0)	0.19	0.56	0.54	0.06	0.32	0.010	26 (1.5)
4	MHQ[8,9]	*n*-BuOH	*n*-BuOH (2.3)	0.40	0.11	0.45	0.014	0.12	0.0032	63 (0.7)
								0.007	0.0007	
	zwitterion[9]	*n*-BuOH	*n*-BuOH	1.0	7.5×10^{-4}					
				−0.40	0.11	−0.45	0.014	−0.12	0.0032	
5	MHQ[8]	H_2O	H_2O (~1.0)	0.56	1.41	0.53	0.35	0.02	0.018	10 (0.5)
6	MHQ[8]	D_2O	D_2O	0.56	0.44 (3.2)	0.46	0.15 (2.3)	0.01	0.0001	12
	MHQ[8]	MeOH	MeOH	0.21	0.71	0.46	0.12	0.35	0.03	
7	MHQ[8]	MeOD	MeOD	0.25	0.52 (1.4)	0.62	0.054 (2.2)	0.14	0.005	
8	MHQ[8]	EtOH	EtOH	0.39	0.48	0.50	0.07	0.13	0.013	
9	MHQ[8]	EtOD	EtOD	0.11	0.57	0.60	0.07	0.30	0.013	

			Polyhyperbolic Approximation (Eq 12)							
	*AH (*M)	B (Q)	solvent (η/cP)	A_1	k_1 (γ_1)[a] (ps^{-1})	A_2	k_2 (γ_2)[a] (ps^{-1})	A_3	R_Q (nm)	D (nm^2 ps^{-1})
4	MHQ[8,9]	*n*-BuOH	*n*-BuOH (2.3)	0.3	0.14 (0.025)	0.55	0.017 (0.003)			
				0.15	0.004 (0.0007)	0.001	0.0006 (0.0001)			
10	PeH[10]	$PhNMe_2$	$PhNMe_2$[a] (1.41)	0.22	1.2 (0.21)	0.78	0.20 (0.033)			
11	PeCN[10]	$PhNMe_2$	$PhNMe_2$[a] (1.41)	1.02	2.4 (0.40)					
12	$PeCH_3$[10]	$PhNMe_2$	$PhNMe_2$[a] (1.41)	1.00	0.12 (0.021)					
13	$PeCH_2$−OH[10]	$PhNMe_2$	$PhNMe_2$[a] (1.41)	0.20	1.0 (0.18)	0.80	0.15 (0.027)			
14	PeH[11]	TCNE (0.08 M)	MeCN[a] (0.35)	0.06	0.10 (0.017)			0.94	1.05	0.003
15	PeH[11]	TCNE (0.64 M)	MeCN[a] (0.35)	0.44	0.26 (0.043)			0.61	1.03	0.003

[a] τ_L = 15 ps for $PhNMe_2$ and 0.5 ps for MeCN.

dx.doi.org/10.1021/jp507390r | J. Phys. Chem. B 2015, 119, 2444−2453

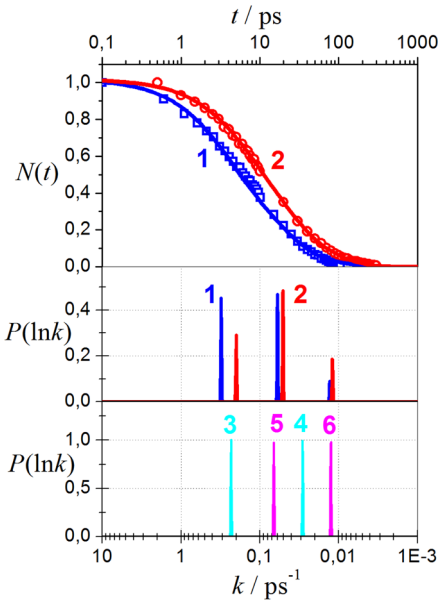

Figure 2. Kinetics of excited-state protolytic dissociation of *MHQ in methanol (**1**, blue) and ethanol (**2**, red; top panel). Fitting by eq 14 is shown by solid lines. Rate distribution functions $P(\ln k)$ for this reaction in methanol (**1**, blue) and ethanol (**2**, red) according to eq 16 for polyexponential approximation (middle panel). Rates of dielectric relaxation ($1/\tau_D$, **3**, **5**) and diffusion ($k_{Diff} = 4\pi R_{Diff} D$, **4**, **6**) in methanol (**3**, **4**, cyan) and ethanol (**5**, **6**, magenta) are shown in the form of narrow Gaussian functions (bottom panel).

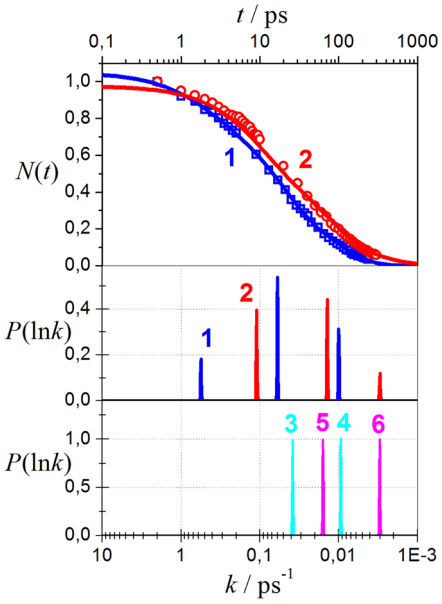

Figure 3. Kinetics of excited-state protolytic dissociation of *MHQ in *n*-propanol (**1**, blue) and *n*-butanol (**2**, red; top panel). Fitting by eq 14 is shown by solid lines. Rate distribution functions $P(\ln k)$ for this reactions in *n*-propanol (**1**, blue) and *n*-butanol (**2**, red) according to eq 16 for polyexponential approximation (middle panel). Rates of dielectric relaxation ($1/\tau_D$, **3**, **5**) and diffusion ($k_{Diff} = 4\pi R_{Diff} D$, **4**, **6**) in *n*-propanol (**3**, **4**, cyan) and *n*-butanol (**5**, **6**, magenta) are shown in the form of narrow Gaussian functions (bottom panel).

different power-law asymptotic tails for the naphthol ($1/t^{3/2}$) and naphtholate ($1/t^{1/2}$), arising from competition between reversible and irreversible geminate reprotonation of naphtholate anion.[23,24] These power-law asymptotic tails can be

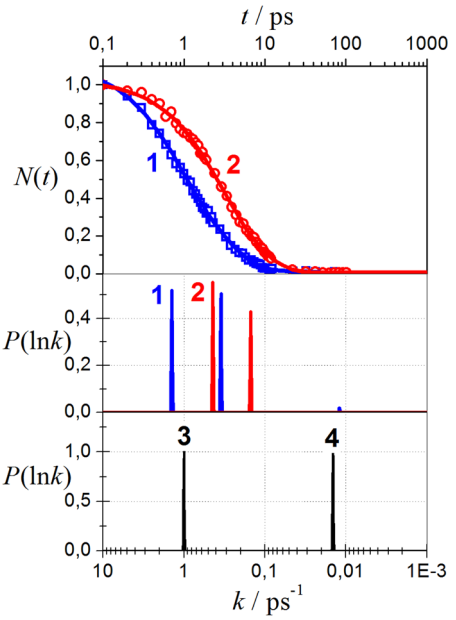

Figure 4. Kinetics of excited-state protolytic dissociation of *MHQ in H_2O (**1**, blue) and D_2O (**2**, red; top panel). Fitting by eq 14 is shown by solid lines. Rate distribution functions $P(\ln k)$ for this reactions in H_2O (1, blue) and D_2O (**2**, red) according to eq 16 for polyexponential approximation (middle panel). Rates of dielectric relaxation ($1/\tau_D$, **3**) and diffusion ($k_{Diff} = 4\pi R_{Diff} D$, $R_{Diff} = 0.5$ nm, **4**) in H_2O are shown in the form of narrow Gaussian functions (bottom panel).

observed at long-times of $t > 10$ ns when geminate reprotonation controls total decay of the excited species. This reprotonation mechanism implies that the proton can undergo a diffusional motion in a rather large volume ($R \sim 10$ nm) possibly only in polar solvents. At $t < 3$ ns, the decay of *5CN2OH and its photodissociation kinetics follow ordinary monoexponential kinetics with $k = 1.1$ ns^{-1}. In the case of *MHQ in BuOH, the lifetime of the zwitterion is too short (~1.3 ns), and geminating the recombination is hidden by the signal noise since the concentration of *MHQ decreases already at $t > 3$ ns by more than 10^3 times. Besides, BuOH has a rather low polarity ($\varepsilon = 17.1$) to allow the proton to move so far from the parent anion. The effect of the counteranion (nonaflate) on the dynamics of the diffusion-limited protolytic photodissociation of *MHQ was discussed by some of us in ref 9. We have performed extensive Brownian dynamics simulation of a three-body zwitterion−proton−counteranion system to reveal the nature of the nonstationary interaction potentials and to elucidate the role of a counteranion in the diffusion and reactivity of the proton in reprotonation of the zwitterion. These simulations show that the counteranion slows down the reprotonation of the zwitterion substantially.

Both the geminate reprotonation and proton−counteranion interaction affect the kinetics of the reaction product predominantly at $t > 1$ ns and cannot be responsible for the observed deviations of PT kinetics from a monoexponential law and extremely large values of $k > 1/\tau_D$ at $t < 1$ ns. For this reason we considered another possibility, a nonuniform solvent shell structure and dependence of the local basicity of the primary proton acceptor−solvent (BuOH) molecules, on the distance between the counteranion that can affect the primary deprotonation rate. Figure 1B demonstrates that $P(\ln k)$ contains main peak at $k_2 \approx 0.02$ ps^{-1}, which practically

dx.doi.org/10.1021/jp507390r | J. Phys. Chem. B 2015, 119, 2444−2453

coincides with the rate of dielectric relaxation $1/\tau_D = 1/63$ ps^{-1} and can be attributed to proton abstraction from *MHQ by regular solvent (BuOH) molecules. One can expect that electrostatic field of the counteranion enhances the basicity of BuOH molecules involved in the solvent shell of the counteranion and attribute the component of $P(\ln k)$ with $k_1 \approx 0.1$ ps^{-1} to proton abstraction by BuOH molecules involved into the solvent shell of the counteranion. Since this $k_1 \approx 0.1$ ps^{-1} exceeds $1/\tau_D$ substantially this reaction should have very small activation energy (~0.1 eV) or proceed by a proton tunneling mechanism.

The estimated difference in activation energies between k_1 and k_2 is about 0.05 eV and can be explained by the difference in the electrostatic interaction with the counteranion in BuOH (ε = 17.1) at the distance of 2 nm. Counteranions located initially at longer distances have to diffuse inside the solvent shell of *MHQ to promote the proton abstraction, and $k_3 \approx 0.003$ ps^{-1} is expected to be related to the diffusion rate coefficient for *n*-BuOH at R_{Diff} = 0.7 nm ($k_{Diff} = 4\pi R_{Diff} D$, where D = 0.0004 nm^2 ps^{-1}).[9] Thus, the major rates of these three components can be attributed to different initial positions of the nonaflate counteranion inside the solvent shell of *MHQ at the moment of the photon absorption. The rate of the slowest component of *MHQ decay ($k_4 \approx 0.0007$ ps^{-1}, $A_4 \approx 0.001$) is close to the rate of the zwitterion decay (τ'_0 = 1.3 ns) and can be attributed to the excited-state equilibrium between the *MHQ cation and zwitterion. One should take into account that this $P(\ln k)$ for initial compound decay cannot contain terms with negative amplitudes ($A_i < 0$, which could be attributed to backward reprotonation) even for reversible reactions since a system always approaches equilibrium from one side and $[RO^-][HS^+]/[ROH][S] < K_{Eq}$. Nevertheless, one can estimate the backward reprotonation rate coefficient from the amplitude of this component A_i, which is close to the ratio of backward and forward reaction rate coefficients: $A_4 \approx k_{-4}/k_4 \approx 0.001$, which corresponds to $pK_a = -3$ for an equilibrium where a protonated solvent molecule is located in the solvent shell of the nonaflate (Nf^-) anion $^{*+}ROH + SNf^- \rightleftarrows {}^{*+}RO^- + HS^+Nf^-$, free energy of ESPT $\Delta G_{PT} \approx -0.17$ eV and $k_{-4} \approx 0.1$ ns^{-1} (which is much smaller than estimations of k_a in ref 8).

For the decay of *MHQ in MeOH, EtOH, and PrOH, several components are observed (see Figures 2 and 3 and Table 1) that also can be attributed to proton abstraction from *MHQ by solvent molecules located in the solvent shell of the counteranion (0.2–0.6 ps^{-1}), by regular solvent molecules (0.05–0.06 ps^{-1}), and to rate of the diffusion of the counteranion (0.010–0.013 ps^{-1}). The values of the diffusion controlled k_3 in MeOH, EtOH, and *n*-PrOH correspond to some greater radius of the solvent shell where the diffusion of the counteranion or proton occurs ($R \approx 1.0$–1.5 nm) than in less polar *n*-BuOH.

These examples of ultrafast ESPT reactions demonstrate that a competition of several mechanisms of PT occurs in reactant pairs which have different initial conditions. Gradual transformations of the dominant mechanism of ESPT can be illustrated by Figure 5 where partial rates of *MHQ decay in BuOH ($-dN_i(t)/d(\ln t)$) for each fraction are plotted vs time. One can see that at t < 20 ps the reaction can be attributed to proton abstraction by the solvent molecules of the solvent shell of the counteranion with k = 110 ns^{-1}. In the time domain 0.02 < t < 0.3 ns PT is controlled by the rate of the medium reorganization (k = 14 ns^{-1}) and can be attributed to proton abstraction by regular solvent molecules. In the time domain

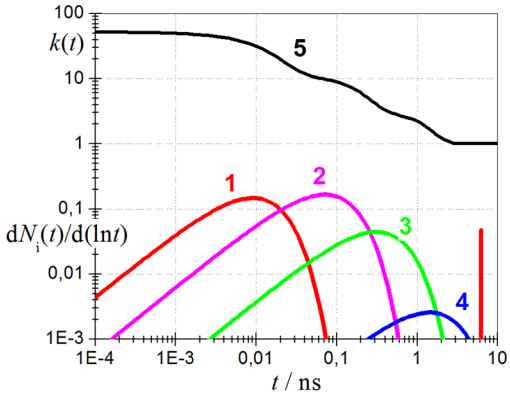

Figure 5. Transformations of *MHQ decay mechanism in BuOH: (**1**, red line) proton abstraction by BuOH molecules from the solvent shell of counteranion initially located close to OH group of *MHQ ($k > 1/\tau_D$); (**2**, magenta line) proton abstraction by regular BuOH molecules of the solvent controlled by the medium reorganization ($k = 1/\tau_D$); (**3**, green line) diffusion of the counteranion inside the solvent shell of *MHQ to its OH group ($k = k_{Diff}$); (**4**, blue line) equilibrium decay of the zwitterion and *MHQ ($k = 1/\tau'_0$). Time-dependent *MHQ decay rate coefficient ($k(t) = \sum_i A_i k_i \exp(-k_i t)/\sum_i A_i \exp(-k_i t)$) is shown by the black line (**5**).

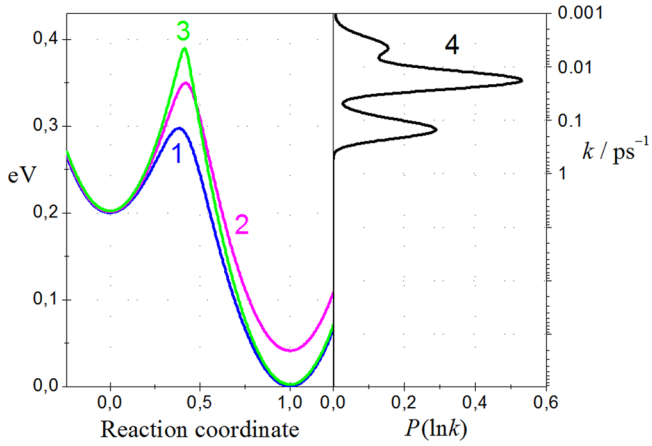

Figure 6. Schematic diagram of potential energy curves (**1**–**3**) for excited-state PT (left panel) and distribution of rates $P(\ln k)$ (**4**; see Figure 1) for *MHQ in *n*-butanol (right panel). Blue line **1** corresponds to proton abstraction by solvent molecules of the solvent shell of counteranion connected by H-bond with OH group of *MHQ ($k > 1/\tau_D$); magenta line **2** corresponds to proton abstraction by regular BuOH molecules of the solvent controlled by the medium reorganization ($k = 1/\tau_D$); green line **3** corresponds to diffusion of the counteranion inside the solvent shell of *MHQ to its OH group ($k = k_{Diff}$). The relationship of PT rate coefficient and activation energy was supposed to be $k = (k_B T/h) \exp(-\Delta G^{\ddagger}/RT)$.

0.3 < t < 2 ns PT is controlled by the rate of the counteranion diffusion. And finally at t > 2 ns the rate of *MHQ decay is controlled by the rate of its zwitterion decay (k = 0.7 ns^{-1}, τ'_0 = 1.3 ns).

Figure 6 shows a schematic diagram of two potential curves for PT in the excited electronic state of this H-bonded complex with BuOH molecules located in the solvent shell of the counteranion and regular BuOH molecules corresponding to k_{PT} = 0.11, and 0.014 ps^{-1} (obtained in polyexponential approximation of PT kinetics) and third potential curve for PT controlled by the diffusion of the counteranion (k_{PT} = 0.003 ps^{-1}). The right panel shows the experimental distribution $P(\ln$

dx.doi.org/10.1021/jp507390r | J. Phys. Chem. B 2015, 119, 2444–2453

k) obtained by a polyhyperbolic approximation. It seems that a continuous distribution corresponds better to the physical behavior of the solvation.

ESET Kinetics. Several examples of ESET reaction kinetics in a neat electron donating solvent are shown in Figures 7 and 8. Their descriptions in the form of the distribution functions $P(\ln k)$ for polyexponential decay (eqs 14 and 16) and for polyhyperbolic decay (eqs 12 and 13, $A_3 = 0$) are given in the middle part of these figures. For ET reactions, a polyexponential description of excited molecular decay in a general case cannot provide rate coefficients which can be attributed to definite physical parameters of the reaction or medium. For instance, the decay of *PeMe (3-methylperylene) and *$PeCH_2OH$ (3-methanolperylene) in neat $PhNMe_2$ is described by triexponential functions where two exponents in fact belong to the single band of the distribution $P(\ln k)$.

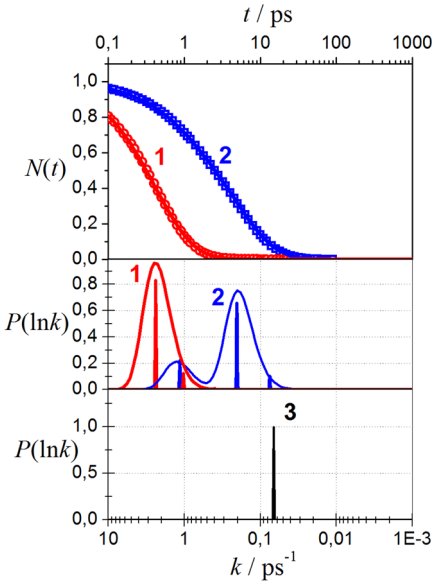

Figure 7. Kinetics of *PeCN (**1**, red) and *PeH (**2**, blue) decay in neat $PhNMe_2$ (according to experimental data[10]; top panel). Distributions $P(\ln k)$ for poly exponential approximation (eqs 14 and 16) of this kinetics (narrow Gaussian red (*PeCN, **1**) and blue (*PeH, **2**) curves) and for Laplace transform (eqs 12 and 13, $A_3 = 0$; red (*PeCN) and blue (*PeH) curves; middle panel). Longitudinal relaxation time (τ_L = 15 ps) of $PhNMe_2$ is shown by black narrow Gaussian curve (**3**; bottom panel).

Rather wide distribution of electronic coupling matrix element in liquid solutions related to strong fluctuations of distances between reactant molecules and their mutual orientations[7,16−18] results in wide distribution of rates. For this reason the description of ET reactions in terms of continual rate distributions is more correct than polyexponential description.

Rather wide distributions of electronic coupling matrix element $P(\ln V^2)$ caused by fluctuations of V in liquid solutions were obtained by quantum chemistry and molecular dynamics calculations of Castner et al.[16] and Scherer[17,18] for single pairs of reactant molecules in the interior of the solvent shell (R_{AD} < 0.9 nm) for coumarin 152 and oxazine in neat $PhNMe_2$. These $P(\ln V^2)$ can be described by Gaussian distribution with $V^2_{max} \approx 2 \times 10^{-5}$ eV^2 and $\sigma \approx 3$. But more narrow distribution $P(\ln(\sum_n V_n^2))$ with the value of V^2_{max} 2 orders of magnitude higher (V^2_{max} = 0.0015 eV^2, $\sigma \approx 0.5$) was

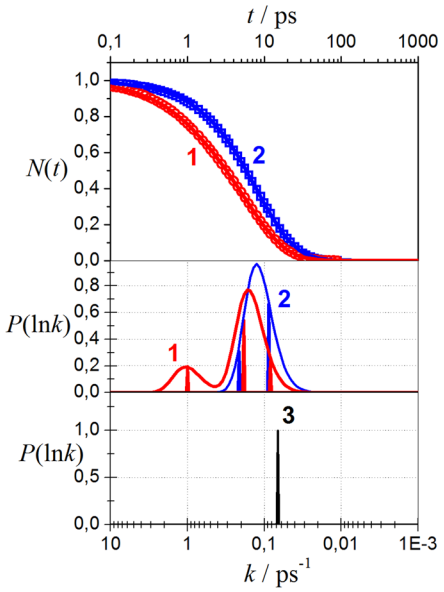

Figure 8. Kinetics of *$PeCH_2OH$ (**1**, red) and *$PeCH_3$ (**2**, blue) decay in neat $PhNMe_2$ (according to experimental data;[10] top panel). Distributions $P(\ln k)$ for polyexponential approximation (eqs 14 and 16) of this kinetics (narrow Gaussian red (*$PeCH_2OH$, **1**) and blue (*$PeCH_3$, **2**) curves) and for Laplace transform (eqs 12 and 13, A_3 = 0; red (*$PeCH_2OH$) and blue (*$PeCH_3$) curves; middle panel). Longitudinal relaxation time (τ_L = 15 ps) of $PhNMe_2$ is shown by black narrow Gaussian curve (**3**; bottom panel).

obtained in the same work of Scherer[17] for a sum of V^2 for all electron donor molecules, located in the first solvation layer (the overall V^2; Figure 9). The width of this distribution $P(\ln(\sum_n V_n^2))$ is close to the width of the experimental distributions $P(\ln k)$. For this reason, the ET reaction rate should be considered as controlled by total electronic coupling with all reactant molecules located inside the solvation layer rather than by pair interactions with some of these molecules.

One can estimate Franck−Condon factor, F_{FC}, for the radiationless mechanism of ET by comparing total value of $\int_{0.0001}^{0.01} \sum_n V_n^2 dV^2$ = 0.0017 eV^2 obtained from quantum chemistry and molecular dynamics calculations of Scherer[17] with experimental values of k_{ET} = 1−2.4 ps^{-1} for the radiationless mechanism of ET for perylene, its derivatives and coumarins in neat $PhNMe_2$. According to the standard expression for rate of ET controlled[25] by electronic coupling matrix element, V_{AD}, and Franck−Condon factor, F_{FC}, $k_{ET} = (4\pi^2/h)\, V_{AD}^2 F_{FC}$, where h is a Plank constant, one obtains F_{FC} = 0.15 eV^{-1}. Close values of $F_{FC} \approx 0.1$−0.3 eV^{-1} were obtained from the experimental parameters of ET for various charge separation and charge recombination reactions with $\Delta G_{ET} \approx -(0.5-1.2)$ eV.[26,27] Thus, the fast fraction of the experimental distribution $P(\ln k)$ with $k_1 \approx 1-5$ ps^{-1} can be attributed to the activationless radiationless transition (nonadiabatic) mechanism of ET (involving internal vibrational modes of the reactant molecules), controlled by the sum $\sum_n V_n^2$ to all electron donor molecules located inside the first solvation layer, rather than by preliminary medium reorganization.

The reactant molecules which have no optimal mutual orientation in the ground state prior to the photoexcitation to provide sufficient values of $\sum_n V_n^2$ (~0.001−0.01 eV^2) require some preliminary reorganization of the medium to react and have $k_2 < 1$ ps^{-1}, close to $1/\tau_L$ of the medium (τ_L is longitudinal relaxation time).

dx.doi.org/10.1021/jp507390r | J. Phys. Chem. B 2015, 119, 2444−2453

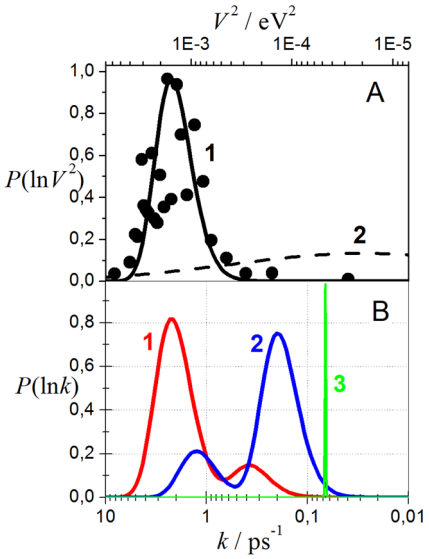

Figure 9. Distribution of overall electronic coupling matrix element (a sum of V^2 to all electron donor molecules, located in the interior of the solvent shell), $P(\ln(\sum_n V_n^2))$, for oxazine in neat *N*,*N*-dimethylaniline[17] (points and solid line **1**) and distribution function for the fluctuations of V^2 for single pairs of reactant molecules in the interior of the solvent shell[17] (dash line **2**; A). Experimental distributions of ET rate coefficients $P(\ln k)$ for coumarin 152 (red line **1**) and perylene (blue line **2**) in neat $PhNMe_2$ (B). Longitudinal relaxation time of $PhNMe_2$ τ_L is shown in the form of narrow Gaussian function (green line **3**). The scale of the panel (A) for V^2 corresponds to the scale of the bottom panel for k at F_{FC} = 0.15 eV^{-1}.

In mixtures of an electron donating solvent with inert solvents a decrease of both rates k_1 and k_2 and of the amplitude of fast component, related to the electronic coupling rate control, occurs (Figure 10). For instance, for coumarin 151 in

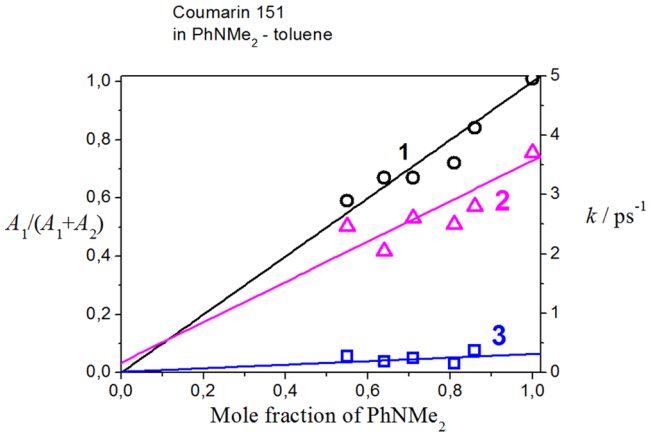

Figure 10. Dependence of the amplitude A_1 (**1**, black circles, left scale), and ET rate coefficients k_1 (**2**, magenta triangles) and k_2 (**3**, blue squares, right scale) for coumarin 151 on mole fraction of $PhNMe_2$ in mixtures $PhNMe_2$–toluene (according to experimental data[16]).

the mixtures of $PhNMe_2$ with toluene $k_1 = k_0(1 + sf_Q) \approx 0.17(1 + 20f_Q)$, where f_Q is a mole fraction of $PhNMe_2$. This dependence confirms that the ET rate depends on total electronic coupling of excited molecule with all quencher molecules located inside the interior of the solvent shell rather than on the rate coefficient of ET in single pairs of reactant molecules, since the number of quencher molecules inside the interior of the solvent shell is proportional to their mole fraction in total solution. From this dependence one can estimate the number of solvent molecules located inside the interior of the solvent shell as about 20, which is close to the estimation of this value $s \approx 13-16$ given in ref 10 for a similar system. The amplitude A_1 is also proportional to f_Q: $(A_1/(A_1 + A_2) \approx 1.0\, f_Q)$ and the total decay rate decreases faster than linearly with the decrease of the quencher concentration.

At small concentrations of the quencher ET reactions become diffusion controlled and their kinetics follows a nonstationary diffusion-controlled regime (eq 12). In this case the distribution $P(\ln k)$ can be described by eq 13. Figure 11 shows $N(t)$ and $P(\ln k)$ for quenching of excited perylene by

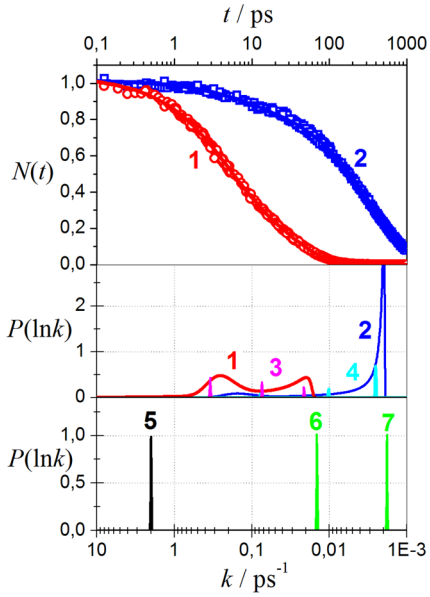

Figure 11. Kinetics of *PeH decay in MeCN in the presence of tetracyanoethylene (0.64 (**1**, red) and 0.08 M (**2**, blue); according to experimental data[11]) and its fitting by eq 12 (top panel). Rate distrubutions $P(\ln k)$ obtained from these data according to combination of hyperbolic decay and nonstationary diffusion (eq 13), **1** and **2**; and in polyexponential approximation (eq 14), **3** and **4**; for these concentrations of TCNE (0.64 M: **1**, red; **3**, magenta; and 0.08 M: **2**, blue; **4**, cyan; middle panel). Longitudinal relaxation time of MeCN (τ_L = 0.5 ps, **5**) and stationary diffusion rates $4\pi R_Q D$[TCNE] at [TCNE] = 0.64 and 0.08 M are shown by narrow Gaussian functions by green lines **6** and **7**, respectively (bottom panel).

different concentrations of tetracyanoethylene in MeCN. One can see two bands which describe two fractions of *PeH which undergo the reaction inside the interior of the solvent shell ($k \sim 0.1-0.3$ ps^{-1}) and diffusion controlled reaction ($k < 0.05$ ps^{-1}) with $R_Q \approx 1$ nm.

Comparison of ESPT and ESET Kinetics. Application of the rate distribution approach to kinetics of several kinds of ultrafast ESPT and ESET reactions in liquid solutions provided a possibility to reveal important similarities as well as dissimilarities between these reactions. In both kinds of reactions different mutual orientations of reactant molecules before photon absorption can result in an appearance after photon absorption of several fractions of reactant pairs with different values of rate coefficients. At the same time, substantial differences in their kinetics exist due to formation in the ground state sufficiently stable H-bonded complexes in

dx.doi.org/10.1021/jp507390r | J. Phys. Chem. B 2015, 119, 2444–2453

the case of PT reactions in contrast to rather weak interactions between reactant molecules in the ground state in the case of ET reactions (we do not discuss here ET which occurs at the excitation in CT band of stable CT complexes). Ground state H-bonded complexes usually have a formation energy of about 0.2−0.3 eV and a definite structure that causes a rather narrow distribution $P(k)$ and exponential kinetics of ESPT in such complex.

In contrast, in ET reactions one observes usually rather wide distribution $P(k)$ ($\sigma \sim 0.4$) and nonexponential kinetics related to fluctuations of the electronic coupling matrix element V_{AD} in the reactant pairs and some nonhomogeneity of the solvent shell. On this reason PT reactions can be described adequately by multiexponential kinetics (or by a set of δ-functions in terms of $P(k)$), but kinetics of ET reactions requires the use of some wider distributions $P(k)$. Different physical behavior is also observed for mutual orientations of reactant molecules before photon absorption. In PT reactions rate coefficients depend first of all on the nature (basicity or acidity) of the reactant or solvent molecule which forms ground-state H-bonded complex and several primary proton acceptors (or proton donors) can exist in real solutions. In ET reactions usually only one kind of primary electron donor (or acceptor) exists, but its orientation and solvent shell can vary depending on some intermolecular interactions with another reactant and solvent molecules (dipole moments, etc.), which can affect the electronic coupling matrix element or reorganization energy and cause an appearance of several fractions with different rate coefficients. Examples of these phenomena were considered above. In some cases a single mode of the decay can be observed even in ET reactions. For instance, the decay of *PeCN (3-cyanoperylene) in neat $PhNMe_2$ can be described by a single band with k_{ET} = 2.4 ps^{-1} (Figure 7). In this case, a strong dipole−dipole interaction between reactant molecules in the ground state provides a predominant orientation of the reactant molecules, which is favorable for strong electronic coupling and very fast ET after photon absorption.[3] One can consider this case as formation of a weak ground state complex between reactant molecules similarly to formation H-bonded complexes in PT reactions.

CONCLUSIONS

Gradual transformations of the mechanism of excited-state PT and ET reactions occur during several nanoseconds due to nonuniform distribution of initial conditions in reactant pairs at the moment of photon absorption. The rate distribution approach provides simple and clear method to reveal these transformations from experimental kinetics using no preliminary hypothesis on the reaction mechanism.

In PT reactions, several kinds of initial H-bonded complexes with different primary proton acceptors or donors can exist. Different basicity or acidity of the primary reactant causes different rate coefficients of PT. Additionally, different distances from the counteranion (i.e., different ΔG_{PT} and pK_a), different diffusion distance, or different solvent shell structure (i.e., different reorganization energy and $\Delta G^{\ddagger}$) can also cause variations of the rate coefficients. Since the structure of these initial H-bonded complexes is rather rigid, each kind of these complexes has a narrow $P(k)$ and total kinetics can be adequately described by polyexponential functions. However, the backward reaction (reprotonation) can also affect total reaction kinetics at longer times (t > 1 ns) due to nonexponential (hyperbolic) kinetics of this backward reaction caused by nonstationary diffusion of proton in the vicinity of primary proton donor anion (in polar solvents where the proton can walk outside the solvent shell of the reactant pair up to 10 nm).

In ET reactions rather wide distribution $P(k)$ is observed even when a single kind of reactant molecules exists in the solution due to wide distribution of electronic coupling matrix element, V_{AD}^2, in the ground state before photon absorption, very fast (∼10 fs) fluctuations of V_{AD}^2 after photon absorption,[16−18] as well as to some distribution of reorganization energies related to the variations of the solvent shell structure. Several mechanisms of ET can be observed for reactant molecules located inside the common solvent shell: radiationless transition mechanism controlled by V_{AD}^2 (when $\Delta G_{ET} < -\lambda$, where λ is total reorganization energy of the medium and reactants) and Marcus mechanism of ET controlled by the reorganization of the medium and reactants. Additionally, nonstationary diffusion control can operate at initial distance between reactant molecules >1 nm. For these reasons, nonexponential kinetics of ultrafast ET is observed practically in all systems.

These differences in PT and ET reactions kinetics should not be considered as fundamental differences in their mechanisms and in fact are related to different conditions used for investigation of these reactions. Ultrafast PT reactions are usually studied in conditions where an H-bonded complex exists between the reactant molecules and the complex is already formed in the ground state prior to the excitation, thus, excluding diffusion effects. In contrast, in the investigations of ET reactions, one usually tries to exclude any ground-state CT complex formation to study real dynamics of ET reaction rather than intramolecular conversions of various excited states of the complex. Similar differences exist also in the conditions for observation of the diffusion effects. In the case of PT reactions nonstationary diffusion can be expected to provide substantial contribution to the reaction kinetics only when very weak H-bonded complexes between reactant molecules are formed and their concentration is less than concentration of free reactant molecules (for instance, in protic solvents with very small basicity). But for ET reactions this nonstationary diffusion almost always complicates the observed kinetics since rates of ET and nonstationary diffusion at $R_{Diff} \approx 1-2$ nm can be comparable (in small viscosity solvents).

ASSOCIATED CONTENT

Related Articles

This is part of our series "Photochemistry of "super" photoacids". For a preceding publication, see: Solntsev, K. M.; Laptenok, S. P.; Naumov, P. *J. Am. Chem. Soc.* **2012**, *134*, 16452−16455.

AUTHOR INFORMATION

Corresponding Authors

*E-mail: kuzmin@photo.chem.msu.ru.
*E-mail: solntsev@gatech.edu.

Notes

The authors declare no competing financial interest.

ACKNOWLEDGMENTS

D.H. acknowledges support by grants from the James-Franck German-Israeli Program in Laser-Matter Interaction and by the Israel Science Foundation. K.M.S. acknowledges generous

support from the National Science Foundation (CHE-1213047). We thank Noam Agmon for helpful discussion.

REFERENCES

(1) *Hydrogen-Transfer Reactions*; Hynes, J. T., Klinman, J. P., Limbach, H.-H., Schowen, R. L., Eds.; Wiley-VCH: Weinheim, 2007; Vol. *1*−*4*.
(2) *Hydrogen Bonding and Transfer in the Excited State*; Han, K. L., Zhao, G.-J., Eds.; Wiley: New York, 2010; Vol. *1*−*2*.
(3) Rosspeintner, A.; Lang, B.; Vauthey, E. Ultrafast photochemistry in liquids. *Annu. Rev. Phys. Chem.* **2013**, *64*, 247−271.
(4) Electron Transfer: From Isolated Molecules to Biomolecules. In *Advances in Chemical Physics: Electron Transfer - from Isolated Molecules to Biomolecules*; Prigogine, I., Rice, S. A., Eds.; Wiley: New York, 2007; Vol. *106*−*107*.
(5) Kosower, E. M.; Huppert, D. Excited state electron and proton transfers. *Annu. Rev. Phys. Chem.* **1986**, *37*, 127−156.
(6) Nitzan, A. *Chemical Dynamics in Condensed Phases: Relaxation, Transfer and Reactions in Condensed Molecular Systems*; Oxford University Press: New York, 2006.
(7) Kuzmin, M. G.; Soboleva, I. V. Analysis of transformations of the ultrafast electron transfer photoreaction mechanism in liquid solutions by the rate distribution approach. *Photochem. Photobiol. Sci.* **2014**, *13*, 770−780.
(8) Gould, E.-A.; Popov, A. V.; Tolbert, L. M.; Presiado, I.; Erez, Y.; Huppert, D.; Solntsev, K. M. Excited-state proton transfer in *N*-methyl-6-hydroxyquinolinium salts: solvent and temperature effects. *Phys. Chem. Chem. Phys.* **2012**, *14*, 8964−8973.
(9) Popov, A. V.; Gould, E.-A.; Salvitti, M. A.; Hernandez, R.; Solntsev, K. M. Diffusional effects on the reversible excited-state proton transfer. From experiments to Brownian dynamics simulations. *Phys. Chem. Chem. Phys.* **2011**, *13*, 14914−14927.
(10) Morandeira, A.; Fürstenberg, A.; Gumy, J.-C.; Vauthey, E. Fluorescence quenching in electron-donating solvent. *J. Phys. Chem. A* **2003**, *107*, 5375−5383.
(11) Pagès, S.; Lang, B.; Vauthey, E. Ultrafast spectroscopic investigation of the charge recombination dynamics of ion pairs formed upon highly exergonic bimolecular electron-transfer quenching: looking for the normal region. *J. Phys. Chem. A* **2004**, *108*, 549−555.
(12) Arnaut, L. G.; Formosinho, S. J.; and Burrows, H. *Chemical Kinetics: From Molecular Structure to Chemical Reactivity*; Elsevier: Amsterdam, 2007.
(13) Zhou, Y.; Zhuang, X. Robust reconstruction of the rate coefficient distribution using the phase function method. *Biophys. J.* **2006**, *91*, 4045−4053.
(14) Steinbach, P. J.; Chu, K.; Frauenfelder, H.; Johnson, J. B.; Lamb, D. C.; Nienhaus, G. U.; Sauke, T. B.; Young, R. D. Determination of rate distributions from kinetic experiments. *Biophys. J.* **1992**, *61*, 235−245.
(15) Angulo, G.; Cuetos, A.; Rosspeintner, A.; Vauthey, E. Experimental evidence of the relevance of orientat. *J. Phys. Chem. A* **2013**, *117*, 8814−8825.
(16) Castner, E. W.; Kennedy, D.; Cave, R. J. Solvent as electron donor: donor/acceptor electronic coupling is a dynamical variable. *J. Phys. Chem. A* **2000**, *104*, 2869−2885.
(17) Scherer, P. O. J. Microscopic models for ultrafast photoinduced solvent to dye electron transfer in DMA/oxazine solution. *J. Phys. Chem. A* **2000**, *104*, 6301−6307.
(18) Scherer, P. O. J.; Tachiya, M. Computer simulation studies of electron transfer parameters for cyanoanthracene/*N*,*N*-dimethylaniline solutions. *J. Chem. Phys.* **2003**, *118*, 4149−4157.
(19) Burshtein, A. I. Non-Markovian theories of transfer reactions in luminescence quenching and photo- and electrochemistry. *Adv. Chem. Phys.* **2004**, *129*, 105−418.
(20) Burshtein, A. I. Contact and distant luminescence quenching in solutions. *Adv. Phys. Chem.* **2009**, Article ID 214219.
(21) Pines, E.; Huppert, D.; Agmon, N. Geminate recombination in excited-state proton transfer reactions: Numerical solution of the Debye-Smoluchowski equation with back-reaction boundary conditions. *J. Chem. Phys.* **1988**, *88*, 5620−5630.
(22) Here and later we chose this representation instead of real δ-function that has infinite amplitude and an area of 1. Gaussian function with amplitude = 1 and area = 1 is rather wide (σ = 1) and inconvenient for the comparison of different $P(\ln k)$ in graphical presentations. To have in the figures narrow peaks convenient for these graphical comparisons, we chose the Gaussian function with σ = 0.005. Since τ_D is also not a constant and some distribution of τ_D exists in various methods of the measurements, it is not misleading to use these narrow Gaussian distributions instead of real δ-functions in all cases.
(23) Solntsev, K. M.; Huppert, D.; Agmon, N. Photochemistry of "super"-photoacids. I. Solvent effects. *J. Phys. Chem. A* **1999**, *103*, 6984−6997.
(24) Solntsev, K. M.; Agmon, N. Dual asymptotic behavior in geminate diffusion-influenced reaction. *Chem. Phys. Lett.* **2000**, *320*, 262−268.
(25) Marcus, R. A.; Sutin, N. Electron transfers in chemistry and biology. *Biochim. Biophys. Acta* **1985**, *811*, 265−322.
(26) Mataga, N.; Taniguchi, S.; Chosrowjan, H.; Osuka, A.; Yoshida, N. Ultrafast charge transfer and radiationless relaxations from higher excited state (S2) of directly linked Zn-porphyrin (ZP)-acceptor dyads: investigations into fundamental problems of exciplex chemistry. *Chem. Phys.* **2003**, *295*, 215−228.
(27) Gould, I. R.; Noukakis, D.; Gomez-Jahn, L.; Young, R. Y.; Goodman, J. L.; Farid, S. Radiative and non-radiative electron transfer in contact radical-ion pairs. *Chem. Phys.* **1993**, *176*, 439−456.